Electrokinetic Streaming Current Methods to Probe the Electrode-Electrolyte Interface Under Applied Potentials

Prantik Saha[1], Changwoo Nam[2], Michael A. Hickner[2], Iryna V. Zenyuk[3,4*]

[1]Department of Physics & Astronomy, University of California Irvine, Irvine, CA 92617, USA

[2]Pennsylvania State University, Department of Materials Science and Engineering, State College, PA, 16801

[3] National Fuel Cell Research Center; Department of Chemical and Biomolecular Engineering, University of California Irvine, Irvine, CA 92617, USA

[4]Department of Mechanical Engineering, Tufts University, Medford, MA 02155

*e-mail: iryna.zenyuk@uci.edu

Abstract: At an electrified interface of metal and electrolyte ion concentration in diffuse layer is different from the bulk and is impacted by metal charge. The double layer structure can significantly enhance local ionic conductivity. Understanding the conductivity enhancement with conventional electrochemical measurements is challenging, however electrokinetic experiments can be more useful in probing local ionic conductivities. We used streaming current experiments for a range of pH values to measure zeta potential at metal-electrolyte interfaces. We extend the method by incorporating a three-electrode electrochemical cell where the potential of the metal can be varied. By using a range of applied potentials between -200 and 800 mV (vs. standard hydrogen electrode) we explored how surface charging of Au electrode affects zeta potential. An inflection point is observed on the plot of zeta potential against applied potential and this point is

believed to be a potential of zero charge of the electrode. Using the Gouy-Chapman-Stern-Grahame model we correlate measured zeta potential values to metal surface charge and calculate ionic distribution and conductivity within the microchannel. Lastly, ionic conductivity is calculated as a function of metal surface charge and as expected from Gouy-Chapman theory shows a parabolic relationship.

1. Introduction

Understanding electric double layers (EDLs) [1] at the electrode-electrolyte interface is critical for electrocatalysis. Potential difference across EDL is the driving force for current density in Faradaic reactions. Electrochemical characterization methods such as cyclic voltammetry and various displacement techniques[2,3] provide information about the surface species and redox reactions as function of applied potential in various acidic, neutral or alkaline environments. These experiments are typically conducted in a three-electrode cell, where the surface of interest acts as a working electrode and two other electrodes act as reference and counter. In such a configuration the potential of zero charge (pzc) of the electrode of interest (such as Au, Pt, Ir) can be measured by observing the sign of the CO-displacement curves, where CO displaces positive or negative ions from the surface, and at a point where the current sign reversal happens, this is considered to be the pzc[4,5]. High ionic strength electrolytes are used to ensure that the EDLs are small (Debye length is ~10 nm order in 1 mM KCl), and most of the potential drop occurs within a few nanometers next to the electrode. In a conventional Gouy-Chapman-Stern theory depicted in Figure 1, for an electrolyte with high ionic strength most of the potential difference occurs between the metal and the outer Helmholtz plane (OHP), which is the plane of the closes approach of solvated ions.

Electrochemical devices such as polymer electrolyte fuel cells (PEFCs), CO_2-reduction reactors, water desalination and nitrogen reduction reactors rely on porous electrodes; with electrocatalyst buried within micro- or meso-pores[6–8]. In the confined environment of the pores water may be the only ion carrier, which has low ionic strength resulting in thick EDLs. Furthermore, local EDL structure under applied potentials is not well understood[9]. It has been reported that ionic conductivity of water in a charged porous matrix may reach 0.001 S/cm[10], which is 5 orders of magnitude higher than the conductivity of the DI water. The local structure and ionic conductivity in the diffuse layer of EDLs cannot be probed with conventional three-electrode electrochemical setup because typically high ionic strength electrolyte is used, which masks the effects of local conductivity.

Electrokinetics and streaming-current/potential experiments have been widely used in colloidal science to probe the EDLs and the electrokinetic potential of the electrode-electrolyte interface. This electrokinetic potential is known as zeta potential, which is generally used to assess the colloidal stability in dispersion[1,11]. The theory was originally developed for colloidal particles but later have been applied to flat extended samples[12,13]. In streaming-current measurements, a pressure difference is applied across a capillary or rectangular slit made of the material of interest and streaming current, which is current at the slip plane is measured as a function of applied pressure. From these measurements Zeta potential can be calculated, which for high concentration of electrolyte, is also the potential at the OHP[14]. Measurements of Zeta potential for metallic surfaces have been challenging due to additional surface conduction[15]. Using streaming-potentials various authors have developed an indirect but complex method to measure Zeta potential for metallic surfaces[16]. The advancement of technology in measuring nano Ampere currents enabled the measurements of Zeta potential directly for conductive surfaces using streaming-current

experiments[17–19]. For example, Roessler et al[20] argued that streaming current experiments on titanium sample is a correct way to measure zeta potential, whereas streaming potential measurements have to be adjusted to correct for surface conductivity. The method has also been extended to measure Zeta potential for ion-conductive membranes, where the surface conductivity is also an issue[13].

Streaming current experiments can probe the EDL structure and local ionic conductivity at metal-electrolyte interface. These experiments can be particularly helpful when combined with standard three-electrode electrochemical set-up to understand the presence of the surface oxides, or other adsorbed species. In this study we have developed a design to measure Zeta potential of metallic surfaces under externally applied potentials to the electrode surfaces. Zeta potential can shed light on the EDLs, whereas three-electrode electrochemical cell can provide data about surface chemistry (adsorption, electrochemical reactions etc). Understanding the double layer structures at different applied potentials will hopefully help us understand the mechanisms of ion transport in water filled electrodes and confinement effects that are relevant for many electrochemical applications.

From electrochemical consideration, cyclic voltammetry experiments give vital information about the oxidation states of the elements, surface adsorptions, oxides formation on the surface and capacitance of the double layers. In addition, experimental techniques, such as electrochemical quartz crystal microbalance[21], surface X-ray scattering[22], and electrochemical scanning tunneling microscopy [23] can be used to correlate surface charge with surface potentials; and theoretical techniques, such as DFT[24] to physically model the electrochemical reactions at the interface. Atomic force microscopy (AFM) has been used to probe the EDLs of metallic surfaces[25] and it can also be used to model some aspects of the double layer (potentials for example) by fitting

the force profile with theoretical model[26]. Previous studies have also attempted to simultaneously measure electrokinetic parameters (e.g. Zeta potential) by both streaming potential methods and AFM measurements[27]. To the best of our knowledge, the approach adopted in our study has not been used before, and it is a first attempt to combine electrokinetic measurements with a three-electrode electrochemical cell to probe the EDLs and ionic conductivity at the metal-electrolyte interface.

In this paper, we discuss the EDL theoretical model, the streaming current method to determine Zeta potential for conductive surfaces, and the design of the three-electrode electrochemical cell incorporated into the electrokinetic set-up. Gold electrodes were chosen due to their electrochemical inertness and large stability window. Using Zeta potential measurements under applied potentials and a range of pH, we calculate the charge distribution and ionic conductivity within the EDLs. Furthermore, we correlate the charge distribution within the electrolyte to the electric charge present within the metal.

2. Theoretical model

2.1. Physics of the Electric Double Layer

When an electrode surface comes in contact with an electrolyte, ions within the electrolyte re-distribute at the electrode-electrolyte interface. The species redistribution at the interface is primarily due to dipole reorientation, and also due to charge separation (i.e. electrons in electrode and ions in electrolyte). If the surface of the electrode is positively charged (due to either adsorbed charge or electric charge) then it will attract negative ions and repel positive ions. In this way, layers of charges of alternate polarity will be formed across the interface. Figure 1 is a schematic

representation of the ion, dipoles and potential distributions according to the Gouy-Chapman-Stern-Grahame (GCSG) model[28–31].

As shown by Figure 1(a), the layer of charges which is in the closest proximity to the electrode surface is called inner Helmholtz plane (IHP). This layer contains two chemical species- one, specifically adsorbed ions with partial or no hydration shield; and two, water dipoles aligned along the electric field in the area[32]. With the strong chemical bond, ions in this layer are unable to stream with the bulk liquid. Further away from the electrode surface, the strength of the electric field and chemical interactions decrease, and ions become mobile. The layer of the mobile ions is termed as the outer Helmholtz plane (OHP) or a shear plane. OHP usually contains the solvated ions held as a result of Coulombic attraction. The electrostatic potential defined in this layer, measured with respect to the potential in the bulk (neutral) electrolyte is called the zeta potential. Figure 1 (b) and (c) show a schematic of typical potential and ion distributions at the interface and bulk electrolyte. When plotting the potential distribution, a moderate ion specific adsorption is assumed.

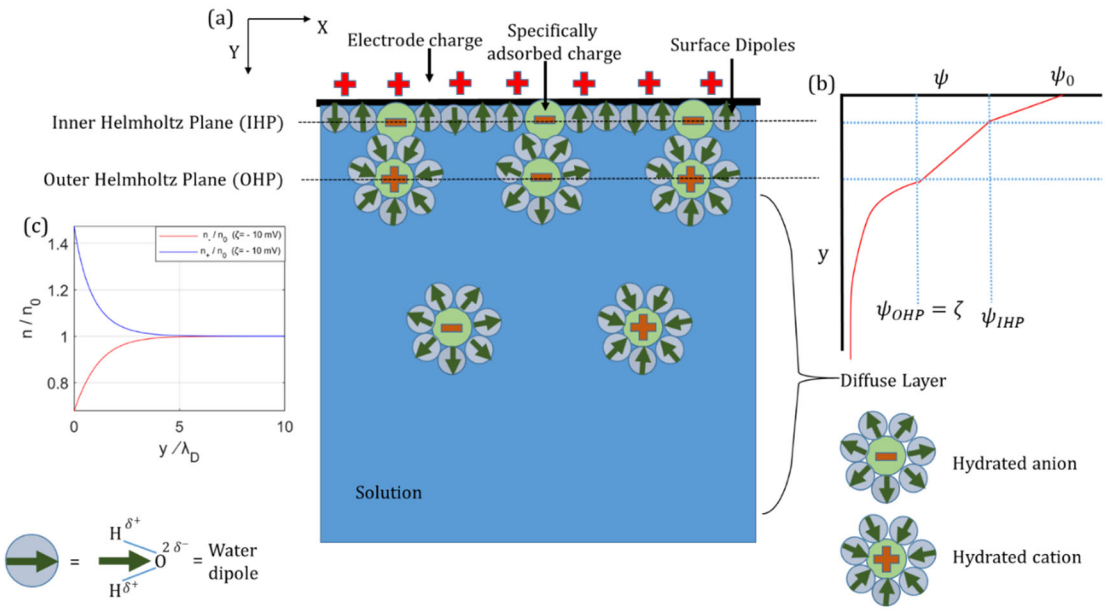

Figure 1: Schematic presentation of the EDLs according to the GCSG model[28–31]: (a) Ions distribution close to the electrode surface, (b) variation of potential from the electrode(c) distribution of ionic fraction outside OHP (for negative Zeta).

In this work, the region of the diffuse layer up to the OHP is of interest. The well-known Gouy-Chapman (GC) theory is conceptually sufficient to describe the region outside the OHP, which we will use as the basis for the stationary EDL model.

2.2 Model Equations

Stationary EDLs: Ion and potential distribution in the diffuse layer

A stationary EDL model describes ion and potential distributions within the 1D micro-channel without the flow of electrolyte. Outside of the shear plane, ion distribution is determined by electrostatic interactions and thermal fluctuations, which can be modelled by the Poisson-Boltzmann (PB) equation. In this section, we present the full solution of the PB equation for our system (10^{-3} M KCl as the electrolyte and 0.01 M HCl and 0.01M NaOH as titrants with a pH

range of 4-10) The setup was a rectangular planar electrode, as shown in Figure 2(b). The PB equations for this geometry can be solved by following Ref[l].

The following approximations were used:

- The electrode, electrolyte and the reservoir are in equilibrium
- Zeta potential is taken to be as an input parameter and taken to correspond to outer Helmholtz Plane (OHP) at y=0
- The system is symmetric along x and z direction. Relevant physical quantities vary along y direction only
- No or weak specific ion adsorption present in the system

The ions in the diffuse layer follow the Boltzmann distribution:

$$n_i(y) = n_i exp\left(-\frac{ez_i\psi(y)}{k_BT}\right) \quad (1)$$

where, $\psi(y)$ is the electrostatic potential at location y, measured with respect to the bulk potential (here bulk is electroneutral, with $\psi = 0$, $n_i(y)$ is the number density of the i^{th} ionic species at y, and k_B is the Boltzmann constant. is the density of the i^{th} ion in the bulk, and z_i is the valency of the i^{th} ion.

The electrolyte contains H^+, K^+ and Na^+ as cations, and Cl^- and OH^- as anions. At position y, the total cationic density:

$$n_+(y) = n_{H^+}(y) + n_{K^+}(y) + n_{Na^+}(y) = ([K^+] + [H^+] + [Na^+])e^{-\frac{e\psi}{k_BT}} = n_+e^{-\frac{e\psi}{k_BT}} \quad (2)$$

where $n_+ = [K^+] + [H^+] + [Na^+]$ is the total density of the positive ions in the bulk. Similarly,

$$n_-(y) = n_{OH^-}(y) + n_{Cl^-}(y) = ([Cl^-] + [OH^-])e^{\frac{e\psi}{k_BT}} = n_- e^{\frac{e\psi}{k_BT}} \quad (3)$$

where $n_- = [Cl^-] + [OH^-]$ is the total density of the negative ions in the bulk.

As the bulk is overall electro-neutral, the number density of positive and negative ions should be equivalent: $n_+ = n_- = n^0$

Poisson-Boltzmann distribution for this system is:

$$\nabla^2\psi = \frac{d^2\psi}{dy^2} = -\frac{\rho_E(y)}{\epsilon_r\epsilon_0} = -\frac{e}{\epsilon_r\epsilon_0}(n_+(y) - n_-(y)) = -\frac{e}{\epsilon_r\epsilon_0}\left(n_+ e^{-\frac{e\psi(y)}{k_BT}} - n_- e^{\frac{e\psi(y)}{k_BT}}\right) \quad (4)$$

where ρ_E is thecharge density, ϵ_r is the dielectric constant of the solution, ϵ_0 is the permittivity of free space. We can partially integrate this non-linear equation[33] to obtain:

$$\frac{d\psi}{dy} = +\left(\frac{2\,k_BT}{\epsilon_r\epsilon_0}\right)^{1/2}\left(n_+\left\{e^{-\frac{e\psi}{k_BT}} - 1\right\} + n_-\left\{e^{\frac{e\psi}{k_BT}} - 1\right\}\right)^{1/2} \quad (5)$$

For our system, the chemical composition in the bulk is shown by Table 1.

Table 1. Concentrations of various ionic species present in the electrolyte.

Chemical species	**Conc. in acidic medium (M)**	**Conc. in basic medium (M)**
K^+	10^{-3}	10^{-3}
Cl^-	$10^{-3} + 10^{-\mathrm{pH}}$	$10^{-3} + 10^{-pH}$
H^+	$10^{-\mathrm{pH}}$	$10^{-\mathrm{pH}}$
OH^-	$10^{-(14-\mathrm{pH})}$	$10^{-(14-\mathrm{pH})}$
Na^+	0	$10^{-(14-\mathrm{pH})}$
n_+	$10^{-3} + 10^{-\mathrm{pH}}$	$10^{-3} + 10^{-(14-\mathrm{pH})}$

n_-	$10^{-3} + 10^{-\mathrm{pH}}$	$10^{-3} + 10^{-(14-\mathrm{pH})}$

Conserving electro-neutrality, we can simplify Eq. (5),

$$\frac{d\psi}{dy} = +\left(\frac{2\,k_B T n^0}{\epsilon_r \epsilon_0}\right)^{1/2}\left(e^{-\frac{e\psi}{k_B T}} - 2 + e^{\frac{e\psi}{k_B T}}\right)^{1/2} = -\left(\frac{8\,k_B T n^0}{\epsilon_r \epsilon_0}\right)^{1/2} sinh\left(\frac{e\psi}{2k_B T}\right) \quad (6)$$

It must be noted that the sign of the right-hand side of the equation cannot be fixed mathematically, as the square root has a sign ambiguity. We have to invoke physical reasoning for the sign. The potential in the bulk is taken to be 0. If $\zeta > 0$, then ψ decreases from $\psi = \zeta$ at y=0 to ψ =0 in the bulk. So, $\frac{d\psi}{dy} < 0$. For $\zeta > 0$, the opposite reasoning applies.

This differential equation can be solved exactly to give the results:

$$tanh\left(\frac{e\psi}{4k_B T}\right) = tanh\left(\frac{e\zeta}{4k_B T}\right)\, e^{-\frac{y}{\lambda_D}} \quad (7)$$

where ζ stands for Zeta potential and $\lambda_D = \left(\frac{\epsilon_r \epsilon_0 k_B T}{2e^2 n^0}\right)^{\frac{1}{2}}$ is the Debye length. For our system (0.001 M KCl), the Debye length is calculated to be 9.72 nm at a room temperature.

For experiment at room temperature (T=300 K), the simplified equation reads (ψ and ζ are in mV):

$$tanh\left(\frac{\psi}{103.2}\right) = tanh\left(\frac{\zeta}{103.2}\right)\, e^{-\frac{y}{\lambda_D}} \quad (8)$$

It can also be rewritten as:

$$\psi(y) = 51.6\, ln\left(\frac{Ce^{\frac{y}{\lambda_D}} + 1}{Ce^{\frac{y}{\lambda_D}} - 1}\right) \quad (9)$$

ψ and ζ are in mV and $C = coth\left(\frac{\zeta}{103.2}\right)$

Substituting Eq. (9) back to Boltzmann Eqs. (2) and (3) one can get the variation of the total number density of both cations and anions, as a function of the distance from the electrode:

$$n_+(y) = n^0 e^{-\frac{ez\psi}{k_BT}} = n^0 \left(\frac{Ce^{y/\lambda_D - 1}}{Ce^{y/\lambda_D + 1}}\right)^2 \text{ and } \quad n_-(y) = n^0 e^{\frac{ez\psi}{k_BT}} = n^0 \left(\frac{Ce^{y/\lambda_D + 1}}{Ce^{y/\lambda_D - 1}}\right)^2 \tag{10}$$

An important corollary of this result is that at OHP, the ratio of cations to anions is:

$$\frac{n_+(0)}{n_-(0)} = e^{-\frac{2ez\zeta}{k_BT}} \tag{11}$$

where for negative ζ, there will be more cations at OHP and for positive ζ, there will be more anions.

Calculating the metal charge from the zeta potential

Gold electrode was used because it's known to be electrochemically inert in the range of applied voltage and pH range of the solution used. There have been prior studies which indicated that towards the higher end of the given potential range and the given concentration, a small amount of chloride adsorption is possible,[34] but we have not found any adsorption peak from the cyclic voltammetry studies, as will be shown in later sections.

By assuming negligible specific adsorption in the IHP the excess charge of the diffuse layer has to be balanced by the charge on the metal surface. For a planar electrode of surface area A, from electro-neutrality:

$$A\sigma_0 + A\int_{OHP}^{\infty} \rho_E(y)dy = 0 \tag{12}$$

where ∞ means the bulk (far from the Debye distance of the diffuse layer), and σ_0 indicates the charge density on the electrode surface. In the above equation, we have already used the fact that

there is no charge in the IHP. The drop of potential from the surface of the electrode to the OHP (Zeta potential plane) is due to the water dipoles and the OHP charges. The fact that adsorbed dipoles can cause a significant drop in the potential is discussed in Ref[32].

We can rewrite the equation, using Poisson's equation,

$$\sigma_0 = -\int_{OHP}^{\infty} \rho_E(y)dy = \epsilon_r\epsilon_0 \int_{OHP}^{\infty} \frac{d^2\psi}{dy^2}dy = \epsilon_r\epsilon_0 \left.\frac{d\psi}{dy}\right]_{OHP}^{\infty} = -\epsilon_r\epsilon_0 \left.\frac{d\psi}{dy}\right]_{y=0} \quad (13)$$

y = 0 has been defined to be the OHP. Now using Eq. (2), and substituting $\psi(0) = \zeta$,

$$\sigma_0 = \epsilon_r\epsilon_0 \left(\frac{8\, k_B T n^0}{\epsilon_r\epsilon_0}\right)^{1/2} sinh\left(\frac{e\zeta}{2k_BT}\right) = (8\, k_B T\epsilon_r\epsilon_0\, n^0)^{\frac{1}{2}}\, sinh\left(\frac{e\zeta}{2k_BT}\right) \quad (14)$$

In the case of no adsorption, we can calculate the surface charge density on the electrode, from the knowledge of the Zeta potential. We insert the values of all the constants to get:

$$\sigma_0 = 11.74\, (n^0)^{\frac{1}{2}}\, \sinh\left(\frac{\zeta}{52}\right)\, \mu C/cm^2 \quad (15)$$

where ζ is in mV. ζ depends on pH and the applied potential on the electrode. n^0 is in mol/L. The above equation can be rewritten in a form, which will be convenient for future use:

$$\sigma_0 = 11.74\, (10^{-3} + 10^{-pH})^{\frac{1}{2}}\, \sinh\left[0.02\, \zeta\left(pH, V_{app}\right)\right] \quad (17)$$

in $\mu C/cm^2$ for acidic medium, while for basic medium, the formula reduces to:

$$\sigma_0 = 11.74\, \left(10^{-3} + 10^{-(14-pH)}\right)^{\frac{1}{2}}\, \sinh\left[0.02\, \zeta\left(pH, V_{app}\right)\right] \quad (18)$$

Electrical conductivity of the double layer

From the knowledge of Zeta potential and hence the ion distribution, one can also predict the conductivity of the double layer. In general, the current density in a solution can be decomposed into the following parts[35]:

$$\vec{j} = -F^2\vec{\nabla}V\sum_i z_i^2 u_i c_i - F\sum_i z_i D_i \vec{\nabla}c_i + F\vec{v}\sum_i z_i c_i \quad (19)$$

The first term is migration, the second term is diffusion and the third term describes convection. F is the Faraday constant ($N_A e \approx 96500\ C/mol$), N_A is the Avogadro number, u_i is the mobility of the ith ion, D_i is the self-diffusion coefficient for ith ion ($D_i = RTu_i$), c_i is the concentration (measured in mol/cm^3) of the ith ion, $\vec{v}$ is the convective velocity, and V is the electrostatic potential.

If the solution is electro-neutral overall, the last term= $\sum_i z_i c_i = 0$. But here for the control volume of interest, the overall electroneutrality within the electrolyte within the channel does not hold. The extra charges are balanced by the charges on the electrode, as seen by the Eq. (14).

In general, when an external electric field is applied inside a micro-channel, two types of ionic velocities arise: migratory and electro-osmotic (convection term). It has been widely discussed that the two velocities are of the same order of magnitude[36,37]. But for the current density, the electro-osmotic velocity must be multiplied with $\sum_i z_i c_i$, where the migratory velocity must be multiplied by $\sum_i z_i^2 u_i c_i$. In the latter case, as z_i^2 is positive, the contributions from all the ions add up. As a result, the contribution from migration is much more dominant than the contribution from convection. So, the 3rd term can be neglected, while calculating the ionic conductivity.

Due to ions distribution within the channel, there is corresponding potential distribution across the channel. If electric field is applied along the x direction, then $V(x,y,z) = V_0 - Ex + \psi(y)$. V_0 is an arbitrary constant related to the reference potential. E is the constant electric field applied externally.

The current density along y is 0 as can be easily seen from the following argument. As the system is symmetric along x and z directions, the ion densities only vary along y:

$$j_y = -F^2 \frac{d\psi(y)}{dy} \sum_i z_i^2 u_i c_i - F \sum_i z_i D_i \frac{dc_i(y)}{dy} = -F \sum_i z_i c_i(y) D_i \left[\frac{F z_i}{RT} \frac{d\psi(y)}{dy} + \frac{1}{c_i(y)} \frac{dc_i(y)}{dy} \right] \quad (20)$$

Where we have used the Einstein relationship: $D_i = RTu_i$. Now, using the facts that $F = N_A e$, $R = N_A k_B$, and $\frac{1}{c_i(y)} \frac{dc_i(y)}{dy} = \frac{1}{n_i(y)} \frac{dn_i(y)}{dy} = \frac{d\{\ln n_i(y)\}}{dy}$, the y component of the current becomes:

$$j_y = -Fk_B T \sum_i z_i c_i(y) D_i \frac{d}{dy} [z_i e\, \psi(y) + k_B T \ln n_i(y)\,] = -Fk_B T \sum_i z_i c_i(y) D_i \frac{d}{dy}\, \bar{\mu}_i(y) = 0 \quad (21)$$

Where $\bar{\mu}_i(y)$ is the net electrochemical potential at y, and for local equilibrium to exist, it should be constant throughout the solution. As a matter of fact, this argument leads to the so-called Poisson-Boltzmann distribution, which is already used here to model the static EDLs.

The current density along Z direction is trivially 0, as it is a direction of symmetry. But the current density along the X direction is non-zero, as a constant electric field E is present. A notation similar to Ohm's law can be adopted:

$\vec{J} = j_x \hat{x} = F^2 \sum_i z_i^2 u_i c_i\, E\hat{x} = \kappa E \hat{x}$ where $\kappa = F^2 \sum_i z_i^2 u_i c_i$ = electrolytic conductance.

From Boltzmann distribution: : $n_i(y) = [n_i] exp\left(-\frac{e z_i \psi(y)}{k_B T}\right) \Rightarrow: c_i(y) = c_i^0 exp\left(-\frac{e z_i \psi(y)}{k_B T}\right)$

where, c_i^0 is the concentration of ions in the bulk. The conductance can be expressed as:

$$\kappa(y) = F^2 \sum_i z_i^2 u_i c_i\,(y) = \frac{F^2}{RT} \sum_i z_i^2 D_i c_i^0 exp\left(-\frac{e z_i \psi(y)}{k_B T}\right) \quad (22)$$

Anionic and the cationic parts can be separated as:

$$\kappa(y) = \frac{F^2}{RT} e^{-\frac{e\psi}{k_B T}} \left(D_{K^+} c_{K^+}^0 + D_{Na^+} c_{Na^+}^0 + D_{H^+} c_{H^+}^0\right) + \frac{F^2}{RT} e^{\frac{e\psi}{k_B T}} (D_{OH^-} c_{OH^-}^0 + D_{Cl^-} c_{Cl^-}^0) \quad (23)$$

Table 2 reports the values of bulk ion concentrations and diffusion coefficients that are substituted into Eq. 23 to calculate ionic conductivity.

Table 2. Diffusion coefficients and bulk concentrations for the ions present in the system.

Ions	$\boldsymbol{c_i^0}$ (mol/l)	$\boldsymbol{c_i^0}$ (mol/cm^3)	$\boldsymbol{D_i}$ x10^5 cm^2/s
H^+	10^{-pH}	$10^{-(pH+3)}$	9.312
OH^-	$10^{-(14-\ pH)}$	$10^{-(17-pH)}$	5.26
K^+	10^{-3}	10^{-6}	1.957
Cl^-	$10^{-3} + 10^{-pH}$	$10^{-6}+10^{-(pH+3)}$	2.032
Na^+	$10^{-(14-\ pH)}$	$10^{-(17-pH)}$	1.334

Note that the values of diffusion constants depend on concentrations of the electrolytes. In dilute solutions values at infinite dilution were taken from literature. All the values are put into Eq. (9), and the variation of conductivity with the distance is expressed as:

$$\kappa(y) = 3.74x10^{-2}\left\{\begin{array}{l}\left(\frac{\coth\left(\frac{\zeta}{103.2}\right)e^{\frac{y}{\lambda_D}}-1}{\coth\left(\frac{\zeta}{103.2}\right)e^{\frac{y}{\lambda_D}}+1}\right)^2\left[1.98x10^{-3}+1.33x10^{-(14-pH)}+9.3x10^{-pH}\right]+\\ \left(\frac{\coth\left(\frac{\zeta}{103.2}\right)e^{\frac{y}{\lambda_D}}+1}{\coth\left(\frac{\zeta}{103.2}\right)e^{\frac{y}{\lambda_D}}-1}\right)^2\left[5.26x10^{-(14-pH)}+2.03x(10^{-3}+10^{-pH})\right]\end{array}\right\} \quad (24)$$

Where the first term is the cationic contribution and the second term is anionic contribution. The conductivity κ, expressed this way, is measured in S/cm, and ζ is in mV. Using this equation, one can plot the variation of κ(y) for different values of $\zeta(pH, V_{app})$ and pH.

Model incorporating fluid flow: Streaming current and Zeta potential

The model is based on a rectangular micro-channel, shown by Figure 2. To measure zeta potential for flat surfaces one can use Helmholtz-Smoluchowski equation[12]. As evident from Figure 2(a), a pressure difference is set up across a micro-channel containing the samples for which Zeta potential is to be measured. The amount of streaming current flowing through the channel is proportional to the pressure difference as well as the Zeta potential of the surfaces.

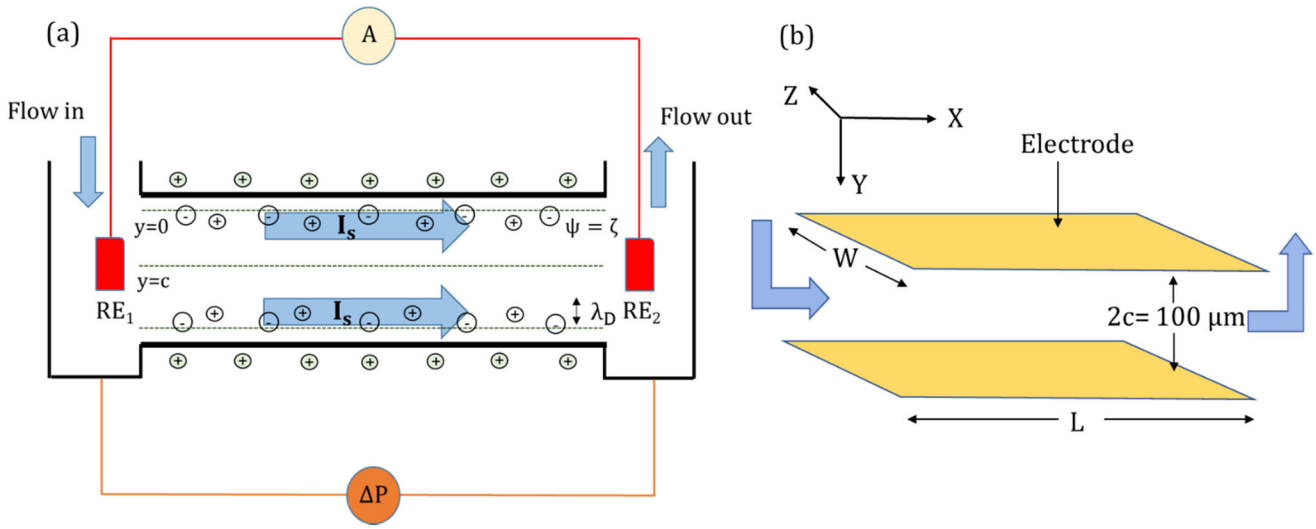

Figure 2: Pressure induced flow and streaming current: (a) Schematic representation (b) Showing the 3D diagram of the electrodes and the channel.

The Navier-Stokes equation for incompressible flow can be written as:

$$\rho\left(\frac{\partial\vec{v}}{\partial t}+(\vec{v}.\vec{\nabla})\vec{v}\right)=-\vec{\nabla}P+\eta\nabla^2\vec{v}+\rho_E\vec{E} \qquad (25)$$

Where, $\vec{v}$ is local velocity of the fluid, P is pressure, η is the dynamic viscosity of the liquid, ρ is density of the liquid.

Model Assumptions:

The Navier-Stokes equations, for rectangular planar geometry has been solved before with the assumptions stated below[38]. The major assumptions used in this study are:

1) Symmetry along X and Z directions make the inertial term $\rho(\vec{v}.\vec{\nabla})\vec{v}=0$.
2) For the system we are considering, $\rho\left|\frac{\partial\vec{v}}{\partial t}\right| \lll \eta\nabla^2\vec{v}$
3) The effect of surface conduction can be avoided for correct measurement of Zeta potential.
4) The effect of the electrostatic force term $\rho_E\vec{E}$, which is along y direction, is negligible.

These approximations 1, 2 and 4 are justified in the Supplementary Material (SM) (a); and the 3rd approximation is shown to be valid in SM (c). After applying the assumptions Eq. (25) simplifies to:

$$-\vec{\nabla}P + \eta\nabla^2\vec{v} = 0 \tag{26}$$

As discussed before, because of the symmetry of the system along x and z direction, the local velocity only depends on y. Written explicitly in terms of Cartesian co-ordinates:

$$-\frac{dP}{dx} + \eta\frac{d^2v_x}{dy^2} = 0 \tag{27}$$

With the boundary conditions: $v_x = 0$ at $y = 0$ and $y = 2c$ (locations of the OHP), the solution reads:

$$v_x(y) = \frac{1}{2\eta}\frac{dP}{dx}y(y-2c) \tag{28}$$

Note that the velocity is opposite to the direction of $\frac{dP}{dx}$ within the range $0 \leq y \leq 2c$ which is consistent. From here, we can calculate the total streaming current (I_s) by:

$$I_s = \int_0^{2c}\rho_E(y)v_x(y)dA = \int_0^{2c}\left(-\epsilon_r\epsilon_0\frac{d^2\psi}{dx^2}\right)\frac{1}{2\eta}\frac{dP}{dx}y(y-2c)Wdy \tag{29}$$

Integrating the system by parts, with the boundary conditions:

$$\psi(y=0) = \psi(y=2c) = \zeta, \psi(y=c) = 0, \frac{d\psi}{dy} = 0 \; at \; y = c$$

and assuming that $\zeta \gg \frac{1}{c}\int_0^c \psi(y)dy$ as potential drops very quickly away from the OHP[39].

The final expression for the streaming current is:

$$I_s = \frac{\epsilon_r\epsilon_0}{\eta}Wd\frac{P}{L}\zeta \Rightarrow \boldsymbol{\zeta = \frac{\eta}{\epsilon_r\epsilon_0}\frac{L}{A}\frac{I_s}{P}} \tag{30}$$

where, A is the electrode surface area and for planar electrodes is defined as width times depth: A = Wd. Note the assumption of no surface conduction. If surface conduction happens, the measured current will be less than the actual current and zeta potential will be under-estimated. The SM sections (c) and (d) show how the situation changes when the surface conduction becomes relevant and how to avoid the part of the data to get the correct estimate of zeta potential.

Furthermore, to reduce the possible errors, we collect the data for more than one pressure value and compute the Zeta potential from the slope of streaming current versus applied pressure:

$$\boldsymbol{\zeta = \frac{\eta}{\epsilon_r \epsilon_0} \frac{L}{A} \frac{dI_s}{dP}} \tag{31}$$

This equation suggests that the streaming current versus pressure curve should be linear, at least at high pressure and in the absence of any surface conduction that might be caused by the Faradaic reactions at the electrode-electrolyte interface. The data for electrically conductive samples should be carefully studied to ensure that these parasitic reactions are minimal and do not affect the slope and zeta potential. SM(c) contains samples of experimental data with data affected by these externalities.

3. Experimental Section

3.1 Standalone Measurement of Zeta Potential

Figure 3 shows the experimental apparatus used in this study. To measure zeta potential of the samples SurPASS Electrokinetic Analyzer 2.0 (Anton Paar, Graz, Austria) was used. The instrument consists of five main components: an external electrolyte container, a pair of pH titration electrolytes (an acid and an alkali), a pair of pressure controllers; and as Figure 3 shows, a measuring cell which contains the micro-channel, and a pair of pressure and electrode sensors.

The streaming current/potential is measured by the reference electrodes. Ag/AgCl electrodes are used for their fast kinetics and due to stability in near neutral pH electrolytes.

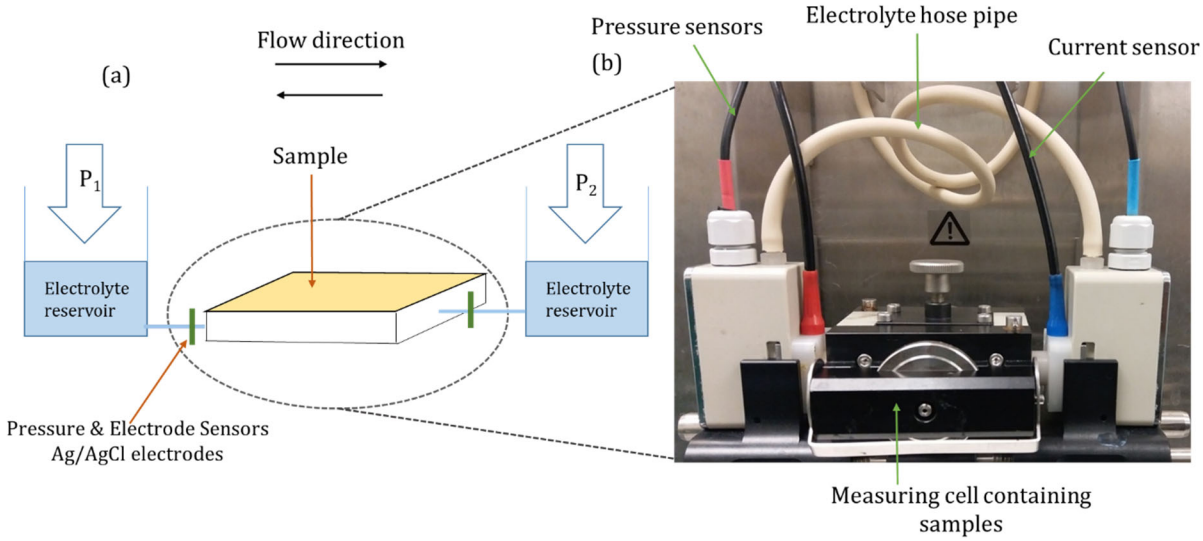

Figure 3: Experimental setup: (a) schematic representation and (b) a photograph of the cell and system components.

The instrument can measure current within the range of ±2 mA, and is calibrated to measure nA range currents, as streaming currents are known to be in the nA range. For example, the highest streaming current we obtained was less than 100 nA. The instrument's working pH range is 2 to 12. The working temperature range is 20° to 40° C. We have selected the pH range of 4-10 and 25°C to ensure stability of the experiment. The cell requires the samples to be cut into dimensions of 20 mm x 10 mm. During the experiment, the gap between the two samples (or the gap of the micro-channel) is kept at 100 µm, which is calibrated with the total measured pressure difference across the channel. As pH titrants 0.01 M HCl and NaOH were used, to ensure small pH changes during titration. The baseline electrolyte used was 1 mM KCl.

The important experimental steps are described here. First, the cell is cleaned with ASTM I grade deionized (DI) water. Then the samples are mounted onto the sample holders and inserted into the micro-channel (shown in Figure 3). The combined channel-hose system is rinsed with 1 mM KCl solution at 400 mbar pressure for 150 seconds. This procedure is to make sure that the air bubbles between the samples get removed. At the same time, the gap between the samples is adjusted to be 100 μm. After this, the actual experimental measurements start. The pH range is set, and the software is pre-programmed to measure zeta potentials for different pH values. For every pH, four experiments are conducted: two of them with the electrolyte flowing in one direction, and the other two with the electrolyte flowing in the opposite direction. The change of flow direction is to ensure that the samples are mounted symmetrically from both sides. For each of the measurements, the pressure is ramped from 0 to 300 mbar and streaming current is measured for each pressure value. As described in the theory section, zeta potential is calculated from the slope of streaming current vs pressure curve. For each pH four zeta values are averaged to get mean zeta potential for a certain pH.

3.2 Measurement of Zeta Potential within the Electrochemical Cell.

To enable measurements of zeta potential of the electrode at applied potentials we developed an electrochemical cell with a three-electrode configuration. Figure 4 shows the schematic and photograph of the electrochemical cell set-up. For this set-up we had electrode surface (here Au) as working electrode (WE), which was the same as that in the previous section. The reference electrode was Ag/AgCl (Pine Instrument Company, Grove City, PA, USA) introduced into the tubing upstream of the flow of electrolyte and the counter electrode was a Pt wire.

Using Ag/AgCl instead of a reversible hydrogen electrode (RHE) served one important purpose- no extra potential difference develops between the reference and the SurPASS 2.0

electrodes (Ag/AgCl electrodes are used as SurPASS 2.0 current sensors). We placed the reference electrode close to the WE to minimize the Ohmic drop through the electrolyte. Ag/AgCl outer diameter is 3.5 mm which made it possible to insert it into the electrolyte stream with minimal intrusion.

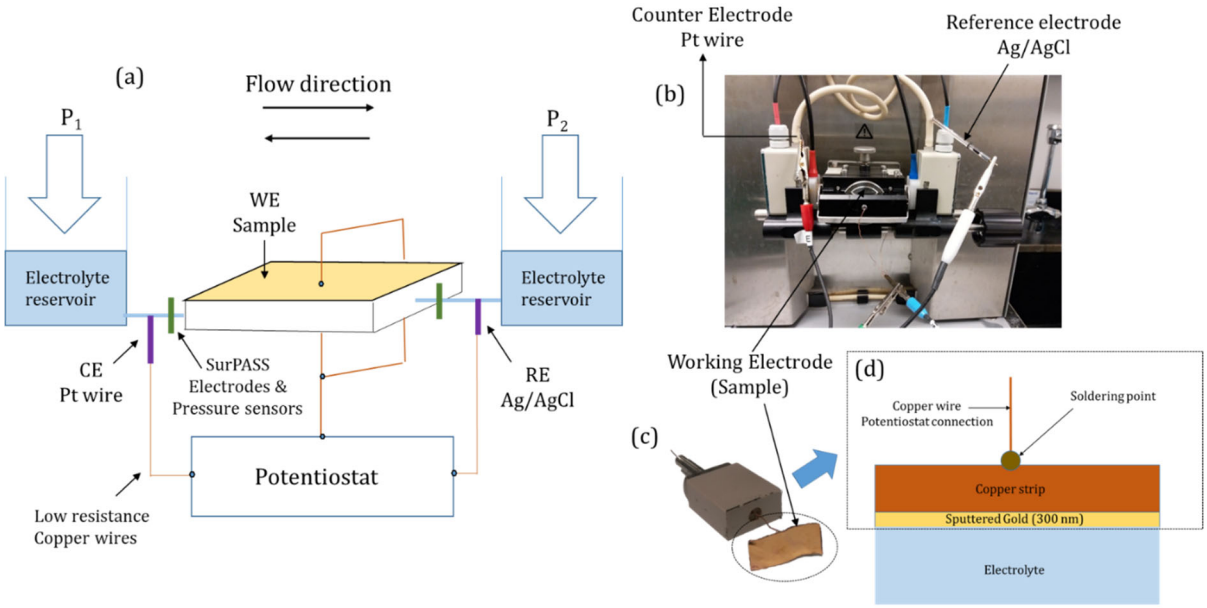

Figure 4: Modified experimental setup with electrochemical cell containing three-electrodes (a) schematic representation, (b) photograph of the actual cell, (c) the modified samples holder with the sample, and (d) The schematic modified sample holder setup

As is evident from the original setup, it is not possible to connect the samples mounted inside the measuring cell to an external circuit. To integrate the sample with external circuit, the sample holder was redesigned as shown by Figure 4(c) and 4(d) to connect an electric wire to the WE. Then a copper wire connected the sample to the working electrode clip of the potentiostat (Gamry Instruments Inc, Warminster, PA, USA). Thus, the working electrode was electrically connected to the potentiostat (Gamry 1010E).

The experimental procedure of data collection was almost identical to the method described in the standalone measurement of zeta potential section, the only difference in this case was the electrodes were held at certain applied potentials. Chronoamperometry experiment was used to apply constant potential. The potentials on the WE were varied from -0.4 V to 0.6 V, at an interval of 0.2 V, with respect to Ag/AgCl electrode. For each fixed potential, the measurement of Zeta potential was done for the pH range of 4-10. The following experimental parameters were set: electrode surface area of 10 mm x 20 mm = 2 cm^2; sampling period (gap between two successive measurements of current) = 0.1 s; maximum current of 0.3 mA. Then the measurements were collected for each applied potential.

3.1. Samples and Preparation Procedure

Au and Ni samples were prepared by sputtering method using NSC Sputter 3000 (Nano-Mater Inc, Austin, TX, USA) machine to deposit Au or Ni onto a thin Kapton film. 300 nm thick layers were deposited by controlling the time of deposition. The deposition of Au and Ni was carried at 7.8 A/s at a power of 150 W. The base pressure of the deposition chamber was $4x10^{-5}$ Torr. For the electrochemical cell Au was sputtered onto a thin film of Cu to ensure good electric conduction between the Au sample and the electrode lead. Pt sample was fabricated by depositing thin-film of Pt onto a 4'' diameter Si wafer by atomic layer deposition (ALD). First, 100 cycles of 10 nm thick aluminum oxide (Al_2O_3) was deposited onto a Si wafer to improve Pt adhesion, followed by 500 cycles of Pt, resulting in 20 nm thick film.

4. Results and discussion

The results section is divided into standalone measurements of Zeta potential for various metallic electrodes and for Zeta potential measurements as a function of applied potentials for Au

electrodes. As mentioned in the previous section, we ran the experiments measuring Zeta potential for several materials, but only for Au, we measured Zeta potential under various applied potentials on the surface of the electrodes. We have varied the applied potential from -200 to 800 mV vs SHE and Au is known to be electrochemically inert in this range[40].

The general observation of decreasing zeta potential with increase of pH has been previously observed[41]. The common interpretation is the accumulation of more cations at the OHP, as is evident from Eq. (11). The complex surface chemistry involved here is beyond the scope of this paper. Instead, the knowledge of Zeta potential under various conditions is used to get quantitative information on some important characteristics like charge on the electrode surface and ionic conductivity within the EDLs.

4.2. Standalone measurement of Zeta potential

Figure 5 shows the comparison of zeta potential measurements of Au sample across the pH range of 4-10. In Figure 5(a), the original set-up measurements of Au deposited on Kapton were almost identical for experiment performed at Tufts University and that at Penn State University in different experiments, indicating the set-up reproducibility and insensitivity to the user handing. We observed some deviation with the data obtained with the modified setup, perhaps because in this case, Au was sputtered onto Cu to make them electrically connectable to an external potentiostat. In Figure 5(b), the data was compared with the data for Au nano-particles[42], and the data obtained for planar Au surfaces by Giesbers et al[27] and Gallardo-Moreno et al[17]. Zeta potential of gold nano-particles was measured by dynamic light scattering method. The nano-particles were synthesized by electrodeposition on porous anodic alumina templates[43]. Particles were approximately 250 nm in diameter and 6 μm long. The electrolyte used was 1 mM NaCl, which is similar to our 1mM KCl. Gallardo-Moreno et al[17] used a gold plate with the streaming current

method. Giesbers et al[27] used streaming potential method which gives rise to erroneous values of zeta potential if not corrected for the surface conduction[12]. Both previous studies used the same electrolyte (1 mM KCl) as used in this study. In this set-up, zeta potential monotonically decreases from -5 mV at pH of 4 to -70 mV at pH of 10. All the values of zeta potential were negative in this pH range. The literature data on the nano-rods also showed decreasing trend but from -35 mV at pH of 4 to -45 mV at pH of 10. The two methods of surface preparation are not identical, and also it is well known that zeta potential depends on the surface geometry[1]. These factors result in the observed differences, but the overall trend is similar. The authors in Ref[27] note that there are no redox reactions present on Au surface within the system of interest (given the electrolyte is N_2 purged) to promote electronic current. The change in zeta potential with pH indicates that H^+ and OH^- participate in the surface charging. Furthermore, negative zeta potential indicates the presence of more cations close to the OHP. With the increase in pH zeta potential becomes even more negative, first leveling off between pH 7 and 9 and then decreasing again above pH 9, suggesting that OH^- forms an oxide layer on the surface of Au, and with increase in OH^- with pH this layer becomes close to a monolayer. This oxide layer has dipole charge attracting H+ to the OHP, decreasing zeta potential values with pH.

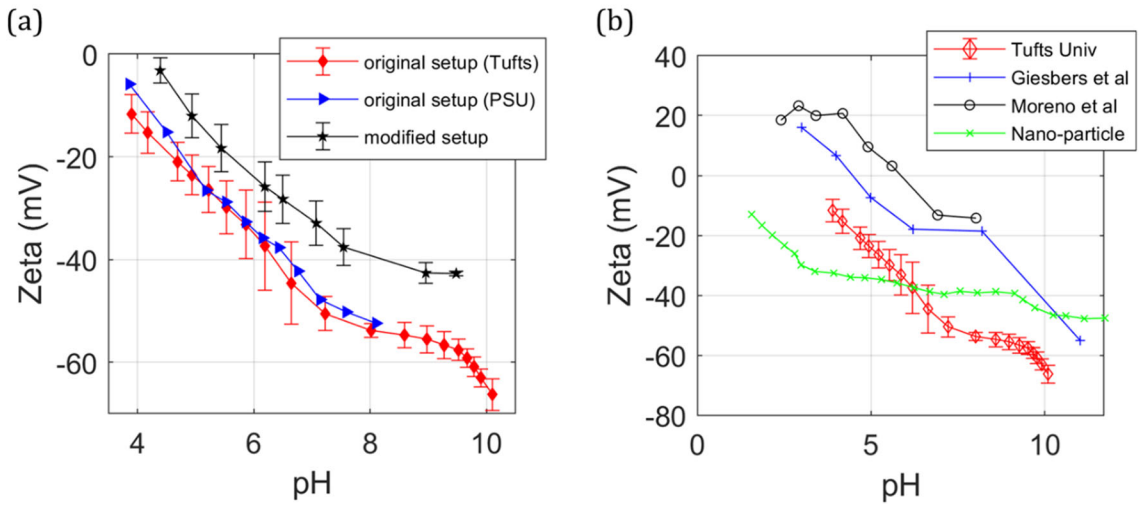

Figure 5: Zeta potential vs pH (a) for original and modified setups and (b) comparison against the published literature data.

Zeta potential values for planar samples of Ni (nickel) and Pt (platinum) with the values found in literature as shown by Figure 6. There is limited literature data of zeta potential as a function of pH for planar metal surfaces[12]. Most of the previous studies used Au as a planar surface due to its inertness in the pH range[40]. The values of zeta potential of Ni powder have been taken from Ref [44]. The authors have used Ni (INCO T-110, Canada) with a mean particle size of 2.5 μm, a surface area of 1 m^2/g and a density of 8.81 g/cm^3. The values of Zeta potential for Pt nano-particles were taken from Ref[45]. The authors produced Pt nano-particles by pulsed laser ablation in liquid of a Pt target. These laser-generated nano-particles had diameters ranging in 3-5 nm.

For both metals, one can see the decrease of Zeta potential with increase of pH. In Ref [45], the authors used the pH range from 1 to 5, while our measurements start at pH 4 (Figure 6a). The sharp drop of zeta potential in the pH range of 4-10 is a significant feature of Pt surface. The drop is also present in case of Pt nano-particles. Again, this can be attributed to oxide formation on the surface of the metals. For both Ni powder as well as Ni surface, one important characteristic is the near-flat behavior of Zeta potential in the pH range of 5-9, indicating that the OHP of the Ni surface has been saturated by ions, and increasing pH does not create any difference (Figure 6b).

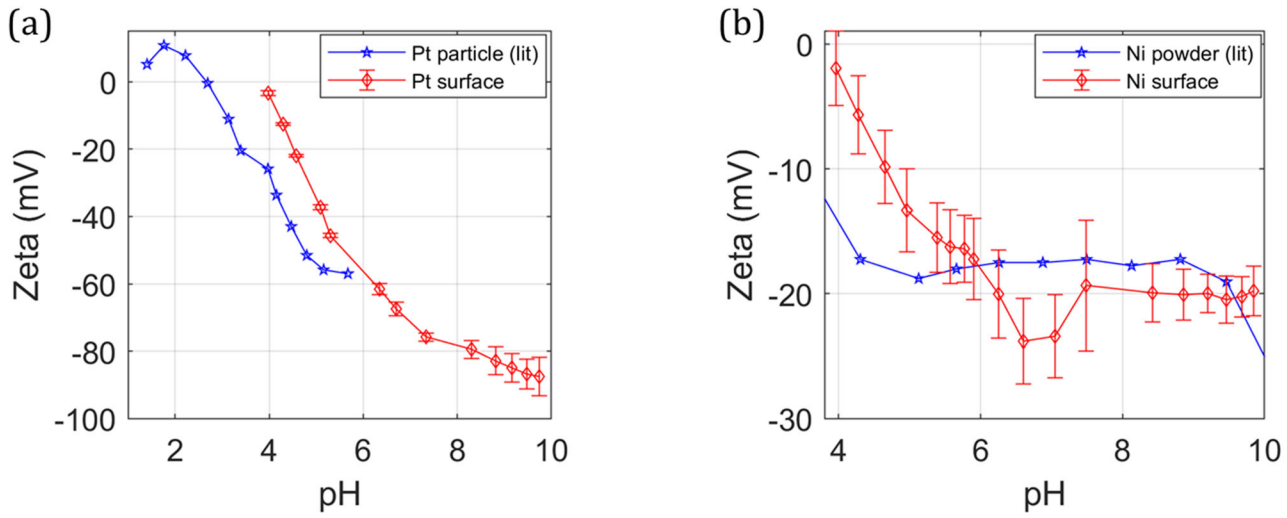

Figure 6: Zeta potential vs pH, with comparison between (a) Pt surface and particles from Ref[45] and (b) Ni surface and particles, Ref[44].

4.3. Measurement of Zeta potential for various electrode applied potentials

Figure 7 shows measured zeta potential for Au electrodes as a function of pH, while the electrodes were held at fixed potentials of -0.4 V, -0.2 V, 0.2 V, 0.4 V and 0.6 V with respect to Ag/AgCl (sat) reference electrode. The conversion between the potential measured with respect to an SHE and that measured with respect to an Ag/AgCl electrode is given by: $E_{SHE} = E_{Ag/AgCl} + 197\ (mV)$. As pH increases zeta potential values decrease for most of the cases studied here. Mostly, for high applied potentials the values of zeta shifted upward indicating higher abundance of negative ions close to the OHP. Essentially, with applied positive potential Au acquires positive charge, as the potentials used here are above the pzc of Au[46–48]. With the positive applied potential, the oxides and adsorbed OH^- are still present on the surface at high pH but they don't completely shield the potential field and OHP gets populated with negative ions. On the other hand, with negative applied potentials and with 0 mV (both below pzc of Au), Au acquires negative charge, negative ions and water still adsorb on the surface, and more protons are present at the OHP to

shield the negative charge on the metal electrode and that introduced by adsorbed dipoles and OH^-

.

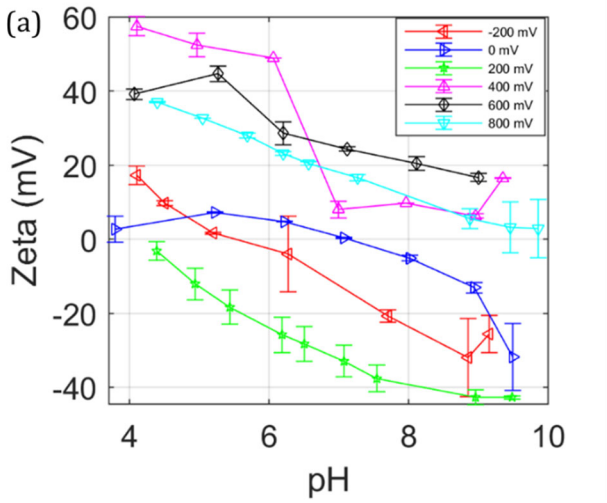

Figure 7: Zeta potential of Au under various applied potentials (with respect to Ag/AgCl)

To understand how applied potential affects zeta potential for a given pH, we plot zeta potential as a function applied potential for three values of pH. Figure 8 shows these plots for applied potentials on the SHE (Figure 8a) and RHE (Figure 8b) scales. We used the conversion scheme from SHE to RHE to be: $E_{RHE} = E_{SHE} + 59 * pH\ (mV)$. On the SHE scale, an inflection point is observed at approximately 300 mV, where Zeta potential increases to higher values. This trend is observed for all three pH values. Again, at a pH of 9, and at applied potentials below 300 mV (vs SHE) Au will be negatively charged, and oxide layer or high degree of coverage of OH^- on the Au surface is present. This renders Zeta potential to be negative between -20 and -40 mV, which is indicative of high concentration of protons at the OHP. For pH 6.5 and for the same applied potentials Au is also negatively charged but smaller ion adsorption occurs due to lower availability of OH^-. Lastly, for pH of 4 we see a small positive Zeta potential values indicative that the OHP has balanced H^+ and OH^- concentrations. For applied potentials above 300 mV (vs SHE)

Zeta potential acquires positive values. At these applied potentials Au is positively charged, and negative ions adsorb on the surface and also are present in the OHP to shield the electric field. At pH 9 more hydroxide ions are present and more are adsorbed on the surface and less are present in the OHP, hence the lower Zeta potential values. All three data sets show an inflection point at 300 mV. To understand this inflection point we translate Zeta potential values into surface charge values using GC theory.

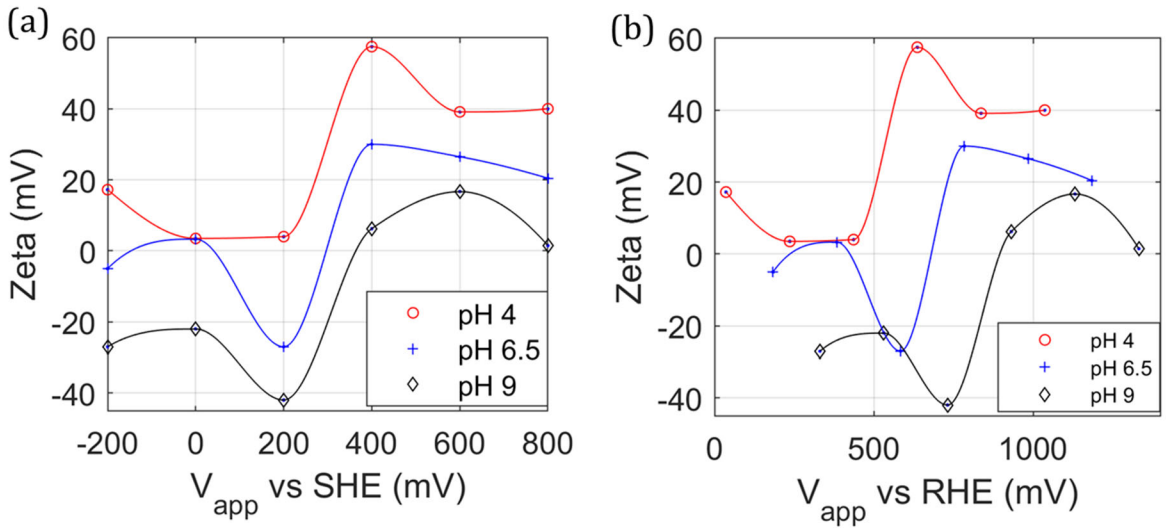

Figure 8: Variation of the Zeta potential of Au with the applied potential on electrode: (a) with respect to SHE, and (b) with respect to RHE.

With the help of Eqs. (17) and (18), we calculate the charge density on the surface of the electrode. Note that these calculations do not include any possible partial charge transfer in the adsorption of OH^-. Figure 9 plots the metal charge density on the electrode surface as a function of pH for applied electrode potentials, measured with respect to Ag/AgCl. Comparing Figure 9 to Figure 7 one can observe direct translation of Zeta potential into surface charge. The trends look very similar, with positive Zeta potential translating into Au positive surface charge. Since Zeta potential values are relatively small, the "sinh" function in Eqs. (17) and (18) can be shown to be

linear in this small Zeta potential values. Therefore, σ_0 is directly proportional to Zeta potential when Zeta is small.

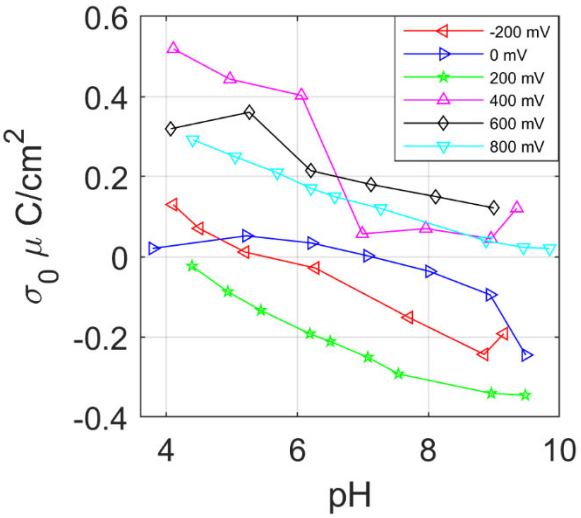

Figure 9. Surface charge density as a function of pH, for applied potentials (vs Ag/AgCl) on Au electrode.

Similarly, we plot surface charge density on Au as a function of applied potential on Au electrode vs SHE. Once again, surface charge density and Zeta potential trends from Figure 8 are similar due to linear behavior of the hyperbolic sine function at small Zeta potential values. Ideally, in the absence of specific adsorption, the charging behavior is expected to be monotonic with respect to the applied potential due to the capacitive effect. However, here at high applied potentials surface charge becomes positive, whereas at potentials <300 mV surface charge on Au is negative for most of the applied potentials and pH values. The pzc of Au has a significant scatter in literature values[47,49,50]. Our results indicate that the pzc is somewhere around the inflection point of 300 mV on the SHE.

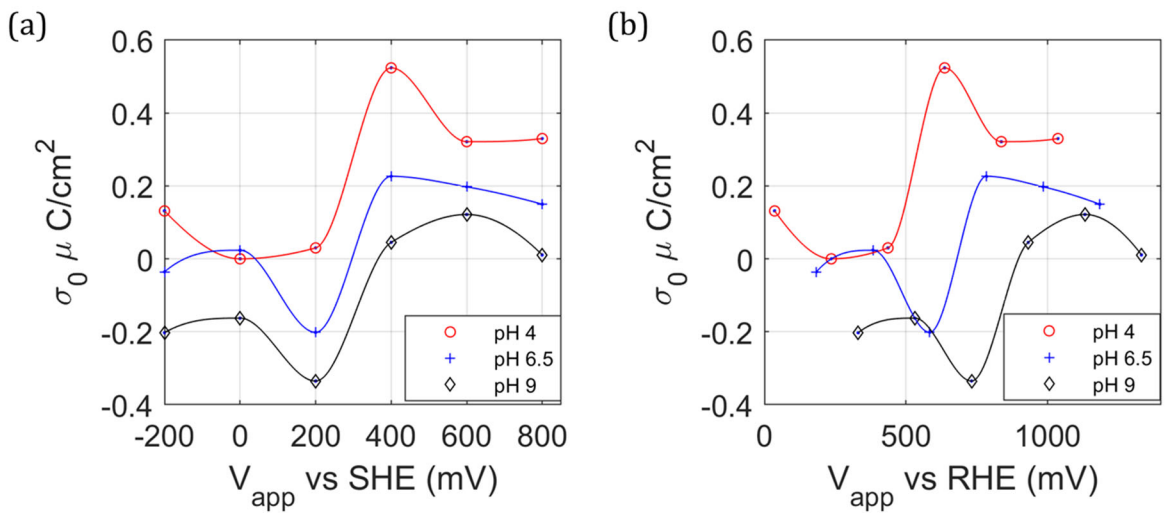

Figure 10. Charge density on the electrode surface as a function of applied potential, at pH 4, 6.5 and 9 (a) with respect to SHE and (b) with respect to RHE.

From the extensive review by Hamelin et al.[51], Au pzc has a complex dependency on the Au crystal structure, types of ions in the electrolyte, pH and concentration. It can be concluded that the Au pzc lies between 200-500 mV with respect to the SHE. Previous studies relied on the thermodynamic methods like electrocapillarity (surface tension and contact angles)[52,53], mechanical methods such as erosion rate[54], scraping methods[48], methods based on double layer capacitance measured by using cyclic voltammetry (CV)[47], AFM[25,55] or ultra-high vacuum work-force measurements[56]. There have been two potential of zero charge terminologies in the literature- potential of zero free charge and potential of zero total charge[3]. In absence of adsorption, these are equal. The choice of electrolyte in this study (1 mM KCl) dictates the presence of adsorption of Cl^- ions, as has been shown to be the case in many studies[4,5]. From the iR corrected CV experiments in the same solution (1 mM KCl), we didn't find any effect of specific adsorption of Cl^- ions on the surface. Therefore, from GCSG theory, we concluded that the charge on the surface of the electrode will balance the charge in the diffuse layer.

Electrochemical charging of gold surface (both 111 single crystal and polycrystalline) has been studied by Climent et al using the laser induced potential transient method[6]. From the current transient analysis of Au(111) in 0.1 M H_2SO_4, they found a reversal in surface charge at an applied potential higher than the known potential of zero charge of Au(111). They argued that this effect is due to the adsorption of SO_4^{2-} on the surface at higher potentials, indicating that it's difficult to separate the effect of adsorption from the free charges of the metal. The decreasing value of surface charge at potentials higher than pzc observed by us (Figure 10) is perhaps due to the adsorption of Cl^- anions on the surface. Hence, the electrokinetic method of determination of surface charge gives information of the total charge on the surface, not the free charge. A more elaborate study of the questions pertaining the effect of electrolyte will be discussed in the follow-up paper. From Figure 10, we also see that the pzc lies between 200-400 mV, but it depends on the pH, as seen by Figure 10b.

Ionic conductivity within the EDLs

One of the advantages of the electrokinetic method is its ability to measure the ionic conductivity. Figure 13 shows ionic conductivity as a function of position 'y' away from the electrode, where $y/\lambda = 0$ is the slip plane and $y/\lambda = 3$ is position away from the slip plane. In the SM Section E, we show that the knowledge of zeta potential fully determines the distribution of ions at the and outside the OHP. The conductivity in the EDL is the highest at the slip plane and drops as one moves away from it. Using Eq. (23), we plot the variation of conductivity from the OHP, for 4 different pH and Zeta potentials, as shown by Figure 11.

We chose the pH and zeta potentials in such a way that the ionic conductivity curves show two distinct trends: fast fall-off and slow fall-off away from the surface. Figure 11 shows that in total, the conductivity varies from 1.5×10^{-4} S/cm to 4×10^{-4} S/cm. As Eq. (23) is a complex function

of ζ and pH, rather than explaining all the curves, let's focus on the pH of 4.5 and pH of 8, which represent Zeta potential of almost equal magnitude (35 and -40 mV, respectively), but different sign and pH values. The conductivities are almost similar. This is expected from the ion distribution shown in Section E of the SM. Having zeta of similar magnitude will attract almost the same number of ions in the diffuse layer; but the mobility of OH^- ions, being less than that H^+ ions, produces slightly lower conductivity at pH of 4.5.

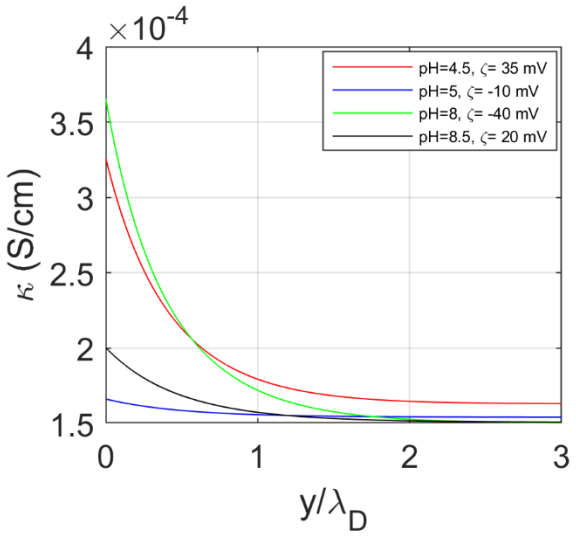

Figure 11. Variation of ionic conductivity within the EDL of Au as a function of distance from the OHP, plotted for 4 different pH and Zeta values.

The bulk conductivity is ≈ 1.47×10^{-4} S/cm (1 mM KCl solution). Note that this value is not dependent on the potential applied to the electrode, as the double layer is thin. The most interesting thing is the conductivity at the slip plane could be as high as four times the bulk conductivity. This is a direct consequence of the formation of the EDLs at the electrode-electrolyte interface, which was also reported in the work of Wang et al[10]. This could have an important

consequence for confined environments and surface-mediated ion transport. Figure 12 shows the plot of the variation of the OHP conductivity with the applied potential for 3 pH values. For the whole applied potential range, the conductivity at the OHP ranges from 1.6 to 8e-4 S/cm. The highest conductivity is achieved at pH of 4 and applied potential of 400 mV vs. SHE. From Figure 10 it can be seen that this is the point at which Au surface has the largest positive surface charge. Therefore, the highest conductivity at pH of 4 is due to high concentration of negative ions. On the other hand, conductivity of the OHP at 600 and 800 mV applied potential is approximately the same at 4e-4 S/cm. From Figure 10 these points correspond to identical surface charge. For pH 9 the peak conductivity is also around 4e-4 S/cm at applied potential of 200 mV, which again from Figure 10 corresponds to the largest negative charge on the Au surface. Interestingly for pH 6.5 ionic conductivity bears almost a flat shape this is because negative and positive charge on the Au electrode alternates between -0.2 and 0.2 $\mu C/cm^2$, which is rather a small range.

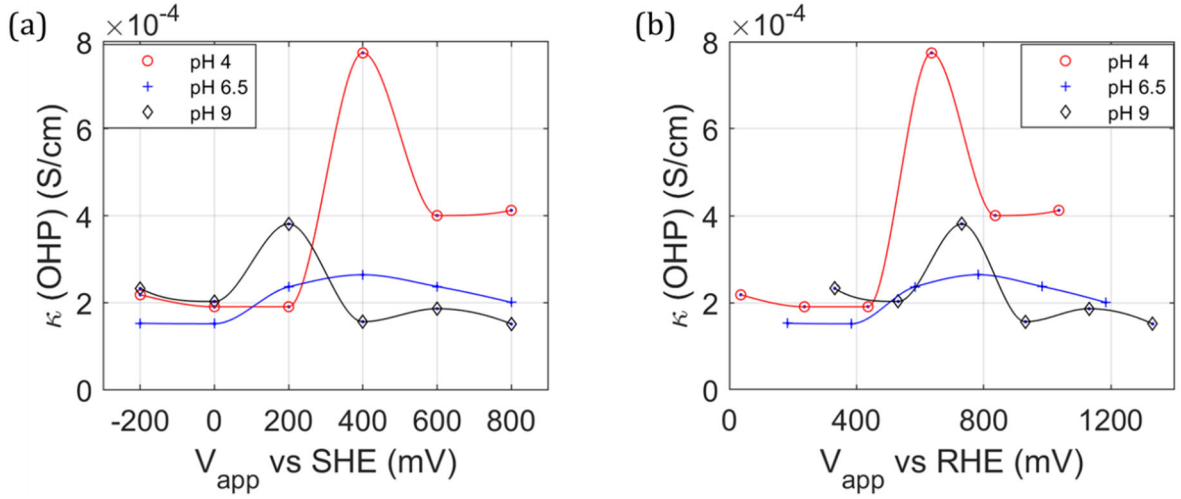

Figure 12. OHP conductivity of Au as a function of different applied potentials, for 3 pH values: (a) with respect to SHE and (b) with respect to RHE

Wang et al. studied how the double layer conductivity of pure water in a charged porous matrix of gold is affected by the applied potential on gold[10]. They found the conductivity to be varying from 1.2×10^{-3} S/cm to $<0.2 \times 10^{-3}$ S/cm when the potential was varied from 0 to 1200 mV vs RHE. The discrepancy between their result and ours could be due to the high electrochemical surface area (~ 150 cm^2) compared to planar surfaces studied here (2 cm^2), as conductivity increases with the electrochemical surface area (ECSA).

Instead of alternatively reading between Figure 12 and Figure 10 we visualize the variation of the ionic conductivity at the OHP for different charge densities on the surface of the electrode, when pH is held constant. Figure 13 shows the parabolic relation between the OHP ionic conductivity and surface charge on the Au electrode. The parabolic relation is predicted by the GC theory. All the points correspond to the applied potential of -200 to 800 mV (vs SHE) applied potential. For pH 4 the Au surface carries mostly positive charge and ionic conductivity varies between 2 and 8e-4 S/cm. At pH 6.5 the Au surface charge is distributed symmetrically about the zero charge point. These conductivities are smaller than those for the other pH values, and are below 3e-4 S/cm. For pH 9 the Au surface charge carries negative charge and conductivity value is at 4e-4 S/cm.

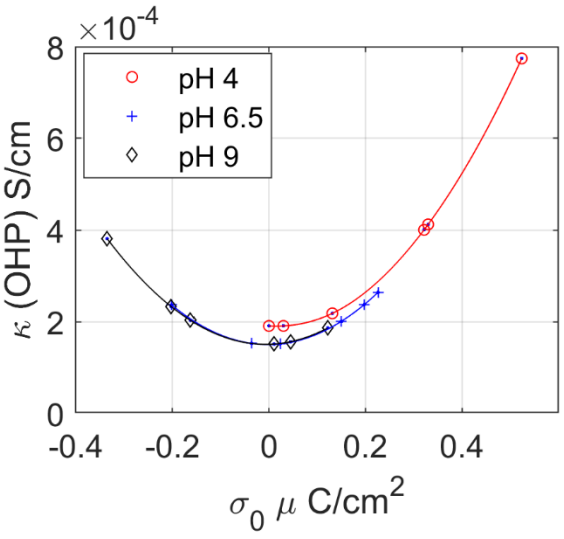

Figure 13. OHP conductivity vs charge density on the electrode surface, for three pH values for the applied potential range of -200 to 800 mV (vs. SHE).

5. Conclusions

In this paper we introduced an experimental method for measuring the zeta potential of electrically conductive surfaces by a streaming current method and extended the method to measure the zeta potential of metal surfaces under applied potentials. Zeta potentials over a range of pH were measured for Au, Ni and Pt, using the streaming current method and the results showed similar trends to literature data using streaming current/streaming potential methods on surfaces and dynamic light scattering methods of particles. Measuring zeta potential of Au for different applied potentials, we deduced some important features of the EDLs: the variation of surface charge density with the pH and applied potential, and the ionic distribution in the diffuse layer. We showed that due to accumulation of ions in the diffuse layer, enhanced conductivity was observed at the OHP. By studying zeta potential at three pHs for applied potential range we show that an

inflection point is observed around 300 mV, above which zeta potential acquires positive value for all three pHs. Positive zeta values indicate accumulation of OH^- ions in the OHP. At higher applied potentials Au is positively charged and OH^- at the OHP shield the electric field. At applied potential below 300 mV at high pHs zeta potential is negative, indicating higher content of H^+ at the OHP. Using the GC theory we correlate zeta potential values for the range of applied potentials with the metal surface charge density. The trends show proportionality between the two values because of small zeta potential values. The highest ionic conductivity values at the OHP are observed for the points where the metal carried the highest charge density (positive or negative). Future studies will explore in-situ cyclic voltammetry correlation with zeta potential.

Supplementary Information

Justifications of the approximations; streaming current vs. streaming potential measurements; back flow of ions and its effect on the evaluation of zeta potential; calculation of zeta potential from the plots that are not fully linear; distribution of ions and variation of potential outside OHP for different Zeta values; comparison with cyclic voltammetry data

Acknowledgements

This work was supported by the National Science Foundation CAREER award 1652445.

6. References

(1) Hunter, R. J. Colloid Science In *Zeta Potential in Colloid Science*; Academic Press, 1981.

(2) Kissinger, P. T.; Heineman, W. R. Cyclic Voltammetry. *J. Chem. Educ.* **1983**, *60*, 702.

(3) Clavilier, J.; Albalat, R.; Gomez, R.; Orts, J. M.; Feliu, J. M.; Aldaz, A. Study of the Charge Displacement at Constant Potential during CO Adsorption on Pt(110) and Pt(111) Electrodes in Contact with a Perchloric Acid Solution. *J. Electroanal. Chem.* **1992**, *330*, 489–497.

(4) Climent, V.; Attard, G. A.; Feliu, J. M. Potential of Zero Charge of Platinum Stepped Surfaces: A Combined Approach of CO Charge Displacement and N2O Reduction. *J. Electroanal. Chem.* **2002**, *532*, 67–74.

(5) Chen, Q.-S.; Solla-Gullón, J.; Sun, S.-G.; Feliu, J. M. The Potential of Zero Total Charge of Pt Nanoparticles and Polycrystalline Electrodes with Different Surface Structure: The Role of Anion Adsorption in Fundamental Electrocatalysis. *Electrochim. Acta* **2010**, *55*, 7982–7994.

(6) Mani, A.; Bazant, M. Z. Deionization Shocks in Microstructures. *Phys. Rev. E* **2011**, *84*, 61504.

(7) Zenyuk, I. V; Litster, S. Modeling Ion Conduction and Electrochemical Reactions in Water Films on Thin-Film Metal Electrodes with Application to Low Temperature Fuel Cells. *Electrochim. Acta* **2014**, *146*, 194–206.

(8) Zenyuk, I. V; Litster, S. Spatially Resolved Modeling of Electric Double Layers and Surface Chemistry for the Hydrogen Oxidation Reaction in Water-Filled Platinum–Carbon Electrodes. *J. Phys. Chem. C* **2012**, *116*, 9862–9875.

(9) Broka, K.; Ekdunge, P. Modelling the PEM Fuel Cell Cathode. *J. Appl. Electrochem.* **1997**, *27*, 281–289.

(10) Wang, Q.; Cha, C.-S.; Lu, J.; Zhuang, L. Ionic Conductivity of Pure Water in Charged Porous Matrix. *ChemPhysChem* **2011**, *13*, 514–519.

(11) Delgado, A. V; González-Caballero, F.; Hunter, R. J.; Koopal, L. K.; Lyklema, J. Measurement and Interpretation of Electrokinetic Phenomena. *J. Colloid Interface Sci.* **2007**, *309*, 194–224.

(12) Werner, C.; Körber, H.; Zimmermann, R.; Dukhin, S.; Jacobasch, H.-J. Extended Electrokinetic Characterization of Flat Solid Surfaces. *J. Colloid Interface Sci.* **1998**, *208*, 329–346.

(13) Xie, H.; Saito, T.; Hickner, M. A. Zeta Potential of Ion-Conductive Membranes by Streaming Current Measurements. *Langmuir* **2011**, *27*, 4721–4727.

(14) Lyklema, J. On the Slip Process in Electrokinetics. *Colloids Surfaces A Physicochem. Eng. Asp.* **1994**, *92*, 41–49.

(15) Hurd, R. M.; Hackerman, N. Electrokinetic Potentials of Bulk Metals by Streaming Current Measurements: I . Method. *J. Electrochem. Soc.* **1955**, *102*, 594–597.

(16) Hurd, R. M.; Hackerman, N. Electrokinetic Potentials on Bulk Metals by Streaming Current Measurements: II . Gold, Platinum, and Silver in Dilute Aqueous Electrolytes. *J. Electrochem. Soc.* **1956**, *103*, 316–319.

(17) Gallardo-Moreno, A. M.; Vadillo-Rodríguez, V.; Perera-Núñez, J.; Bruque, J. M.; González-Martín, M. L. The Zeta Potential of Extended Dielectrics and Conductors in Terms of Streaming Potential and Streaming Current Measurements. *Phys. Chem. Chem. Phys.* **2012**, *14*, 9758–9767.

(18) Zimmermann, R.; Freudenberg, U.; Schweiß, R.; Küttner, D.; Werner, C. Hydroxide and Hydronium Ion Adsorption — A Survey. *Curr. Opin. Colloid Interface Sci.* **2010**, *15*, 196–202.

(19) Chan, Y.-H. M.; Schweiss, R.; Werner, C.; Grunze, M. Electrokinetic Characterization of Oligo- and Poly(Ethylene Glycol)-Terminated Self-Assembled Monolayers on Gold and Glass Surfaces. *Langmuir* **2003**, *19*, 7380–7385.

(20) Roessler, S.; Zimmermann, R.; Scharnweber, D.; Werner, C.; Worch, H. Characterization of Oxide Layers on Ti6Al4V and Titanium by Streaming Potential and Streaming Current Measurements. *Colloids Surfaces B Biointerfaces* **2002**, *26*, 387–395.

(21) Lei, H.-W.; Uchida, H.; Watanabe, M. Electrochemical Quartz Crystal Microbalance Study of Halide Adsorption and Concomitant Change of Surface Excess of Water on Highly Ordered Au(111). *Langmuir* **1997**, *13*, 3523–3528.

(22) Kondo, T.; Morita, J.; Hanaoka, K.; Takakusagi, S.; Tamura, K.; Takahasi, M.; Mizuki, J.; Uosaki, K. Structure of Au(111) and Au(100) Single-Crystal Electrode Surfaces at Various Potentials in Sulfuric Acid Solution Determined by In Situ Surface X-Ray Scattering. *J. Phys. Chem. C* **2007**, *111*, 13197–13204.

(23) Itaya, K. In Situ Scanning Tunneling Microscopy in Electrolyte Solutions. *Prog. Surf. Sci.* **1998**, *58*, 121–247.

(24) Nørskov, J. K.; Rossmeisl, J.; Logadottir, A.; Lindqvist, L.; Kitchin, J. R.; Bligaard, T.; Jónsson, H. Origin of the Overpotential for Oxygen Reduction at a Fuel-Cell Cathode. *J. Phys. Chem. B* **2004**, *108*, 17886–17892.

(25) Wang, J.; Bard, A. J. Direct Atomic Force Microscopic Determination of Surface Charge at the Gold/Electrolyte InterfaceThe Inadequacy of Classical GCS Theory in Describing the Double-Layer Charge Distribution. *J. Phys. Chem. B* **2001**, *105*, 5217–5222.

(26) Barten, D.; Kleijn, J. M.; Duval, J.; Leeuwen, H. P. v; Lyklema, J.; Cohen Stuart, M. A. Double Layer of a Gold Electrode Probed by AFM Force Measurements. *Langmuir* **2003**, *19*, 1133–1139.

(27) Giesbers, M.; Kleijn, J. M.; Cohen Stuart, M. A. The Electrical Double Layer on Gold Probed by Electrokinetic and Surface Force Measurements. *J. Colloid Interface Sci.* **2002**, *248*, 88–95.

(28) Gouy, M. Sur La Constitution de La Charge Électrique à La Surface d'un Électrolyte. *J. Phys. Théorique Appliquée* **1910**, *9*, 457–468.

(29) Chapman, D. L. LI. A Contribution to the Theory of Electrocapillarity. *London, Edinburgh, Dublin Philos. Mag. J. Sci.* **1913**, *25*, 475–481.

(30) Stern, O. Zur Theorie Der Elektrolytischen Doppelschicht. *Zeitschrift für Elektrochemie und Angew. Phys. Chemie* **2018**, *30*, 508–516.

(31) Grahame, D. C. The Electrical Double Layer and the Theory of Electrocapillarity. *Chem. Rev.* **1947**, *41*, 441–501.

(32) J. O'M. Bockris K. Müller, M. A. V. D. On the Structure of Charged Interfaces. *Proc. R. Soc. London. Ser. A. Math. Phys. Sci.* **1963**, *274*, 55.

(33) Baldessari, F. Electrokinetics in Nanochannels: Part I. Electric Double Layer Overlap and Channel-to-Well Equilibrium. *J. Colloid Interface Sci.* **2008**, *325*, 526–538.

(34) Horányi, G.; Rizmayer, E. M.; Joó, P. Radiotracer Study of the Adsorption of Cl− and HSO4− Ions on a Porous Gold Electrode and on Underpotential Deposited Metals on Gold. *J. Electroanal. Chem. Interfacial Electrochem.* **1983**, *152*, 211–222.

(35) Newman, J.; Thomas-Aleya, K. . *Electrochemical Systems*, 3rd ed.; Wiley-Interscience, 2004.

(36) Sadek, S. H.; Pimenta, F.; Pinho, F. T.; Alves, M. A. Measurement of Electroosmotic and Electrophoretic Velocities Using Pulsed and Sinusoidal Electric Fields. *Electrophoresis* **2016**, *38*, 1022–1037.

(37) Nakabe, K. T. and K. N. and K. F. and Y. K. and K. Measurement of Electroosmotic Flow Velocity and Electric Field in Microchannels by Micro-Particle Image Velocimetry. *Meas. Sci. Technol.* **2010**, *21*, 105402.

(38) Burgreen, D.; Nakache, F. R. Electrokinetic Flow in Ultrafine Capillary Slits1. *J. Phys. Chem.* **1964**, *68*, 1084–1091.

(39) Yaroshchuk, A.; Ribitsch, V. Role of Channel Wall Conductance in the Determination of ζ-Potential from Electrokinetic Measurements. *Langmuir* **2002**, *18*, 2036–2038.

(40) Pourbaix, M. *Atlas of Electrochemical Equilibria in Aqeous Solutions*; Pregamon Press, 1966.

(41) Kirby, B. J.; Hasselbrink Jr., E. F. Zeta Potential of Microfluidic Substrates: 1. Theory, Experimental Techniques, and Effects on Separations. *Electrophoresis* **2004**, *25*, 187–202.

(42) G. M. Dougherty J. B.-H. Tok, S. S. Pannu, F. Y. S. Chuang, M. Y. Sha, G. Chakarova, S. G. Penn, K. A. R. The Zeta Potential of Surface-Functionalized Metallic Nanorod

Particles in Aqueous Solution. *UCRL, U.S. At. Energy Comm.* **2007**.

(43) Nicewarner-Peña, S. R.; Freeman, R. G.; Reiss, B. D.; He, L.; Peña, D. J.; Walton, I. D.; Cromer, R.; Keating, C. D.; Natan, M. J. Submicrometer Metallic Barcodes. *Science (80-.).* **2001**, *294*, 137.

(44) Hernández, N.; Moreno, R.; Sánchez-Herencia, A. J.; Fierro, J. L. G. Surface Behavior of Nickel Powders in Aqueous Suspensions. *J. Phys. Chem. B* **2005**, *109*, 4470–4474.

(45) Marzun, G.; Streich, C.; Jendrzej, S.; Barcikowski, S.; Wagener, P. Adsorption of Colloidal Platinum Nanoparticles to Supports: Charge Transfer and Effects of Electrostatic and Steric Interactions. *Langmuir* **2014**, *30*, 11928–11936.

(46) Hamelin, A. The Surface State and the Potential of Zero Charge of Gold (100): A Further Assessment. *J. Electroanal. Chem.* **1995**, *386*, 1–10.

(47) Prado, C.; Prieto, F.; Rueda, M.; Feliu, J.; Aldaz, A. Adenine Adsorption on Au(111) and Au(100) Electrodes: Characterisation, Surface Reconstruction Effects and Thermodynamic Study. *Electrochim. Acta* **2007**, *52*, 3168–3180.

(48) Bode, D. D.; Andersen, T. N.; Eyring, H. Anion and PH Effects on the Potentials of Zero Charge of Gold and Silver Electrodes. *J. Phys. Chem.* **1967**, *71*, 792–797.

(49) Peretz, Y.; Yarnitzky, C. N. Determination of the Pzc at Solid Electrodes with a Dropping Electrolyte Electrode. *J. Electroanal. Chem.* **2001**, *498*, 87–92.

(50) Michri, A. A.; Pshenichnikov, A. .; Burstein, R. K. No Title. *Electrokhimiya* **1972**, *8*.

(51) Hamelin, A.; Lecoeur, J. The Orientation Dependence of Zero Charge Potentials and Surface Energies of Gold Crystal Faces. *Surf. Sci.* **1976**, *57*, 771–774.

(52) Morcos, I.; Fischer, H. Determination of the Potential of Zero Charge from Capillary Liquid Rise on Metal Plates. *J. Electroanal. Chem. Interfacial Electrochem.* **1968**, *17*,

(53) Murphy, O. J.; Wainright, J. S. Determination of Potentials of Zero Charge For Solid Metal/Solution Interfaces. *J. Electrochem. Soc.* **1988**, *135*, 138–143.

(54) Kukoz, F. I.; Semenchenko, S. A. No Title. *Elektrokhimiya* **1966**, *2*.

(55) Hillier, A. C.; Kim, S.; Bard, A. J. Measurement of Double-Layer Forces at the Electrode/Electrolyte Interface Using the Atomic Force Microscope: Potential and Anion Dependent Interactions. *J. Phys. Chem.* **1996**, *100*, 18808–18817.

(56) Lecoeur, J.; Bellier, J. P.; Koehler, C. Comparison of Crystalographic Anisotropy Effects on Potential of Zero Charge and Electronic Work Function for Gold {111}, {311}, {110} and {210} Orientations. *Electrochim. Acta* **1990**, *35*, 1383–1392.

TOC Graphic

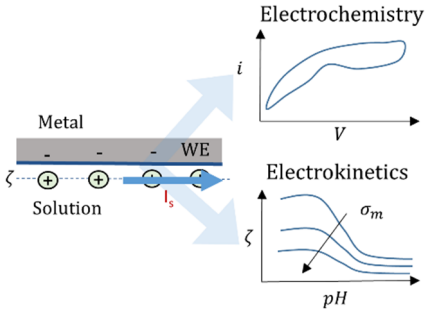
Electrochemistry
i
V
Metal
WE
ζ
Solution
I_s
Electrokinetics
σ_m
ζ
pH